THE ASTROPHYSICAL JOURNAL, 473:L91–L94, 1996 December 20

HUBBLE SPACE TELESCOPE SPECTROSCOPIC EVIDENCE FOR A $1 \times 10^9\ M_\odot$ BLACK HOLE IN NGC 4594[1]

JOHN KORMENDY,[2,3] RALF BENDER,[4] EDWARD A. AJHAR,[5] ALAN DRESSLER,[6] S. M. FABER,[7] KARL GEBHARDT,[8] CARL GRILLMAIR,[9] TOD R. LAUER,[5] DOUGLAS RICHSTONE,[8] AND SCOTT TREMAINE[10]

Received 1996 June 24; accepted 1996 September 24

ABSTRACT

The discovery by Kormendy of a $M_\bullet \simeq 10^9\ M_\odot$ massive dark object (MDO) in NGC 4594 is confirmed with higher resolution spectroscopy from the Canada-France-Hawaii Telescope (CFHT) and the *Hubble Space Telescope* (*HST*). CFHT measurements with the Subarcsecond Imaging Spectrograph improve the resolution from $\sigma_* = 0\farcs40$ to $0\farcs27$ Gaussian dispersion radius of the point-spread function (PSF). The apparent central velocity dispersion rises from $\sigma = 250 \pm 7$ km s^{-1} to $\sigma = 286 \pm 7$ km s^{-1}. As observed with the COSTAR-corrected *HST*, the Faint Object Spectrograph, and a $0\farcs21$ aperture, $\sigma = 321 \pm 7$ km s^{-1} is still higher, and the central rotation curve is very steep. The highest-$M_\bullet$ published dynamical model fits the new observations reasonably well when "observed" at *HST* resolution. The spatial resolution has now improved by a factor of ~5 since the discovery measurements, and the case for a black hole (BH) has strengthened correspondingly.

We confirm that NGC 4594 has a Seyfert spectrum; Hα is ~5200 km s^{-1} wide at zero intensity. However, gas velocities are lower than the circular velocities implied by the stars, so they cannot be used to test the BH case in NGC 4594. The gas may be in a ring, or it may be associated with patchy dust. *HST* images with the Wide Field and Planetary Camera 2 show dust at some aperture positions.

NGC 4594 appears to have a bright point nucleus. However, the central absorption-line strengths are low, consistent with dilution by enough nonthermal light to explain the "nucleus." There is no evidence for a distinct nuclear star cluster. NGC 4594 is similar to M87, which also has a nonthermal nuclear source, and not to M31 and NGC 3115, which have quiescent BHs and nuclear star clusters.

Subject headings: black hole physics — galaxies: individual (NGC 4594) — galaxies: kinematics and dynamics — galaxies: nuclei

1. INTRODUCTION

The COSTAR-corrected *Hubble Space Telescope* (*HST*) is spearheading a new and productive phase in the search for black holes (BHs) in galactic nuclei (see Kormendy & Richstone 1995 for a review). The first galaxy examined via stellar dynamics, NGC 3115, proved to have the largest velocity dispersion seen in any galactic nucleus, $\sigma = 600 \pm 37$ km s^{-1} (Kormendy et al. 1996, hereafter K+96). The ground-based massive dark object (MDO) detection by Kormendy & Richstone (1992) was confirmed. Improved constraints on the radius inside which the dark mass lies also strengthened the conclusion that it is an $M_\bullet \simeq 2 \times 10^9\ M_\odot$ BH.

This paper presents CFHT and *HST* spectroscopy of NGC 4594, the Sombrero galaxy. Based on rapid rotation and a high central velocity dispersion observed with the CFHT at resolution $\sigma_* = 0\farcs40$, Kormendy (1988, hereafter K88) concluded that NGC 4594 contains a BH of mass $M_\bullet \simeq 10^9\ M_\odot$. The kinematics are well confirmed (Jarvis & Dubath 1988; Wagner, Dettmar, & Bender 1989; Carter & Jenkins 1993; van der Marel et al. 1994; Emsellem et al. 1996), as is the dynamical analysis (Emsellem et al. 1994). But no paper has improved the spatial resolution. *HST* improves the resolution by a factor of 5. We show here that this greatly strengthens the BH case. More detailed dynamical models will then be presented in a later paper.

2. CFHT SIS SPECTROSCOPY

The CFHT Subarcsecond Imaging Spectrograph (SIS) was designed for problems like the BH search. The scale is $0\farcs0864$ pixel^{-1}; a slit width of $0\farcs26 \pm 0\farcs01$ was used. Tip-tilt guiding is incorporated; by offsetting the guide probe, we can center the object on the slit to 1 pixel accuracy. An observing sequence consists of a series of direct images to center the object at the slit, an exposure with the slit in place but with no grism, the object spectrum, another image through the slit but without the grism as well as one with neither slit nor grism to verify that the object is still centered, and a comparison spectrum. The results in § 4 are based on the sum of two integrations totaling 70 minutes. The seeing was measured on the bracketing direct images. The brightness profile of the galaxy is the same in these images and in the spectrum, so the PSF in the images is correct for the spectrum. We obtain $\sigma_* = 0\farcs27 \pm 0\farcs01$, or FWHM = $0\farcs63 \pm 0\farcs03$. This is a 33% improvement over $\sigma_* = 0\farcs40$ in K88.

The spectra were taken near the Ca II infrared triplet, at 7975–8975 Å. The reciprocal dispersion was 0.98 Å pixel^{-1} = 34.6 km s^{-1} pixel^{-1}. The $2\farcs5$ slit was too short to let us

[1] Based on observations with the NASA/ESA *Hubble Space Telescope*, obtained at the Space Telescope Science Institute, which is operated by AURA, Inc., under NASA contract NAS 5-26555.

[2] Visiting Astronomer, Canada-France-Hawaii Telescope, operated by the National Research Council of Canada, the Centre National de la Recherche Scientifique of France, and the University of Hawaii.

[3] Institute for Astronomy, University of Hawaii, 2680 Woodlawn Drive, Honolulu, HI 96822.

[4] Universitäts-Sternwarte, Scheinerstrasse 1, München 81679, Germany.

[5] Kitt Peak National Observatory, National Optical Astronomy Observatories, P.O. Box 26732, Tucson, AZ 85726.

[6] Carnegie Observatories, 813 Santa Barbara Street, Pasadena, CA 91101.

[7] UCO/Lick Observatory, University of California, Santa Cruz, CA 95064.

[8] Department of Astronomy, University of Michigan, Ann Arbor, MI 48109.

[9] Jet Propulsion Laboratory, Mail Stop 183-900, 4800 Oak Grove Drive, Pasadena, CA 91109.

[10] Canadian Institute for Theoretical Astrophysics, University of Toronto, 60 St. George Street, Toronto M5S 3H8, Canada.

measure the sky on NGC 4594 spectra, so we used a summed sky exposure taken from several spectra of small objects. This was scaled to the NGC 4594 spectra so that night-sky emission lines subtracted as well as possible.

Velocities and velocity dispersions were calculated with the same Fourier quotient program that was used in K88. Results are averages for four standard stars, η Cyg (K0 III), κ Oph (K2 III), μ Leo (K2 III SMR), and γ Dra (K5 III).

3. *HST* FOS SPECTROSCOPY

NGC 4594 was observed on 1995 February 9–16 with the 0.″21 square aperture and Faint Object Spectrograph (FOS). The aperture was placed along the disk major axis as shown in Figure 1 (Plate L13). At radii r = 0.″032 W, 0.″163 W, and 0.″207 E, the integration times were 178, 228, and 228 minutes, respectively.

The spectra were electronically quarter-stepped, giving 2064, quarter-diode pixels. Flat-fielding and correction for geomagnetically induced motions were done as in K+96. The spectra were then resampled on a log λ scale at a reciprocal dispersion of 1.0837 Å pixel^{-1} = 58.3 km s^{-1} pixel^{-1}. The wavelength range, 4567–6800 Å over 2048 pixels, includes the Mg I b lines at $\lambda \simeq 5175$ Å and the Na I D lines at $\lambda \simeq 5892$ Å. The instrumental velocity dispersion was measured to be FWHM/2.35 = $\sigma_{\rm instr}$ = 1.77 ± 0.03 pixels = 103 ± 2 km s^{-1} (internal error). This is intrinsic to the instrument; it is not strongly affected by how the aperture is illuminated (Keyes et al. 1995). Therefore, aperture illumination corrections to σ are small (see below).

Measured velocities depend on aperture illumination: if a star in the aperture is moved in the dispersion direction, V varies with position by 757 km s^{-1} arcsec^{-1}. The corrections for asymmetrical aperture illumination are larger here than they were for NGC 3115, because the major axis of NGC 4594 was oriented only 13°.2 from the dispersion direction. We corrected for miscentering of the apertures on the galaxy using the final acquisition peak-up intensity array. The apertures were placed at radii 0.″049 W, 0.″162 W, and 0.″204 E of the center (Fig. 1). The luminosity-weighted mean radii are 0.″032 W, 0.″163 W, and 0.″207 E, with estimated errors of about ±0.″003.

Aperture corrections to V and σ were derived as follows. For each FOS spectrum, we divided the 0.″21 aperture into nine slices in the dispersion direction. We calculated the total brightness in each slice from our V-band WFPC2 image. We then velocity-shifted the standard star spectrum appropriately for each slice, multiplied by the brightness in the slice, and added up the results. The sum divided by the total luminosity weight provides, for each aperture position, a standard star spectrum constructed such that the star and the galaxy illuminate the aperture in the same way. These star spectra were used to derive the kinematic results given below. Velocities and dispersions derived as above differ from those given by a standard star centered in the aperture by $\leq$12 km s^{-1} and $\leq$5 km s^{-1}, respectively.

The Mg b lines are contaminated with [N I] 5199 Å emission (Fig. 1). It is tempting to use the Na D lines to measure velocities. But Figure 1 shows dust at some aperture positions. Also, the equivalent width of the D lines is a factor of 2–3 larger than in the comparison star. We conclude that Na D is contaminated by interstellar absorption. Therefore, we measured the kinematics using Bender's (1990) Fourier correlation quotient program on a wavelength region (Fig. 1) that contains Mg b and Fe lines. We removed the emission line in two ways: (1) by interpolating through it and (2) by replacing the affected region iteratively with the broadened and velocity-shifted spectrum of NGC 3379 (Fig. 1). The two procedures give consistent results: σ = 323 ± 22, 320 ± 11, and 312 ± 11 km s^{-1} at r = 0.″032, 0.″163, and −0.″207, respectively. However, the usable wavelength range is much reduced by the emission and interstellar absorption contamination. Therefore V and σ errors are larger than they were in K+96, and line-of-sight velocity distributions cannot be measured.

The new data are illustrated in Figure 2. Also included are measurements by van der Marel et al. (1994) that have much higher signal-to-noise ratios than our data. However, they do not resolve the nuclear disk well, so they are plotted only at $r > 12''$.

4. RESULTS: COMPARISON WITH K88 MODELS

The dynamical components of NGC 4594 show up well in Figure 2 (*left*). NGC 4594 contains a nuclear disk of stars (Fig. 1; Burkhead 1986, 1991; K88; Emsellem et al. 1994, 1996) that is more prominent than the one in NGC 3115 (K+96). It affects the isophotes at $r \lesssim 8''$. At 10″–15″ radius along the major axis, the light is dominated by the bulge, and at still larger radii the main disk takes over. These features are recognizable in the SIS data. At $r \gtrsim 30''$ the kinematics are dominated by the main disk: V is large, and σ is small. Nearer the center, V decreases and σ increases as the bulge contribution increases. By $r \simeq 10''$–12″, the kinematics are purely those of the bulge: σ equals the minor-axis bulge dispersion (K88). Then, at $r < 10''$, the kinematics become those of the nuclear disk. This is quite cold: at $r \simeq 4''$–6″, σ is smaller than the bulge dispersion despite rotational line broadening. At $r \gtrsim 1''$ the rotation curve is resolved (see also Carter & Jenkins 1993). But at $r < 1''$, $V(r)$ and $\sigma(r)$ are so steep that they are unresolved. The rapid central rise in $V(r)$ and the central jump in $\sigma(r)$ are the signature of the MDO.

The MDO case is strengthened by the observation that, as resolution improves, the apparent central kinematic gradients get steeper. The *HST* data imply that already at 0.″14 radius the rotation velocity $V \simeq 110$ km s^{-1}. Similarly, the velocity dispersion gradient gets steeper at better resolution; the apparent central velocity dispersion rises from $\sigma(0)$ = 250 ± 7 km s^{-1} in K88 to 286 ± 7 km s^{-1} in the SIS data and 321 ± 7 km s^{-1} in the *HST* data.

Testing the BH case requires comparison with dynamical models. Making new models is complicated because of the many components; we postpone it to a later paper. However, as in K+96, the BH case can already be checked by comparing published models with the new data.

K88 computed models of NGC 4594, each consisting of an unprojected rotation curve, a velocity dispersion profile, and a volume brightness profile. To prevent the results from being too affected by the composite (hot + cold) stellar population (i.e., by non-Gaussian line-of-sight velocity distributions), the bulge spectrum was subtracted and the nuclear disk was modeled. This removed most of the two-component structure in the line profiles that has been emphasized by van der Marel et al. (1994) and by Emsellem et al. (1996). The residual line profiles were well fitted by the models (Kormendy 1994). Eleven models were constructed; they differed mainly in the steepness of their central kinematic gradients and in their

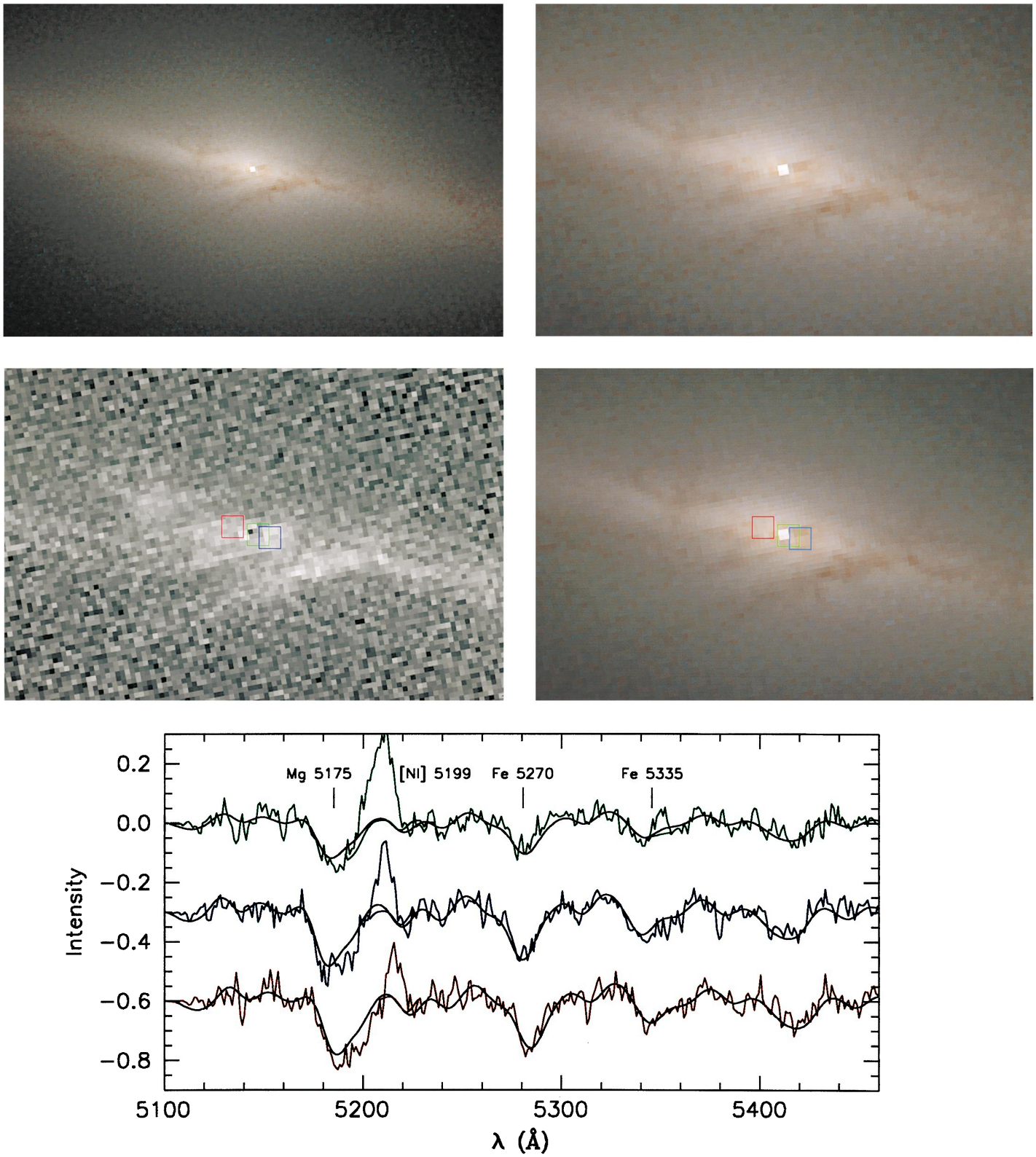

FIG. 1.—(*Top*) *HST* WFPC2 images of NGC 4594. *Upper left*: Color image made from 1200 s *V*-band and 1050 s *I*-band images after 40 iterations of Lucy deconvolution. To emphasize the dust, the image sent to the blue gun of the filmwriter was an extrapolation from *I* through *V*, i.e., I_V^2/I_I, where I_V and I_I are the intensities in *V* and *I*, respectively. This panel is 9.″3 × 6.″2, and the displayed brightness is proportional to the square root of intensity. *Upper right*: Same image expanded by a factor of 2 (4.″6 × 3.″1). *Middle right*: Same as upper right, with the 0.″21 aperture positions superposed. Red indicates the receding side of the galaxy; green and blue indicate the approaching side with respect to the systemic velocity. *Middle left*: Color image $V - I$ coded so that $V - I = 1.6$ is black and $V - I = 2.3$ is white. *Bottom*: Spectra of NGC 4594 in the wavelength region used to determine the absorption-line velocities, color coded as in the images. The spectra are shown before and after the removal of [N I] λ5199. The black lines are the standard star spectrum broadened and velocity-shifted to fit the data. The star spectrum has been scaled using a mean line strength γ; note that the Fourier correlation quotient program is insensitive to the fact that different lines have different γ values.

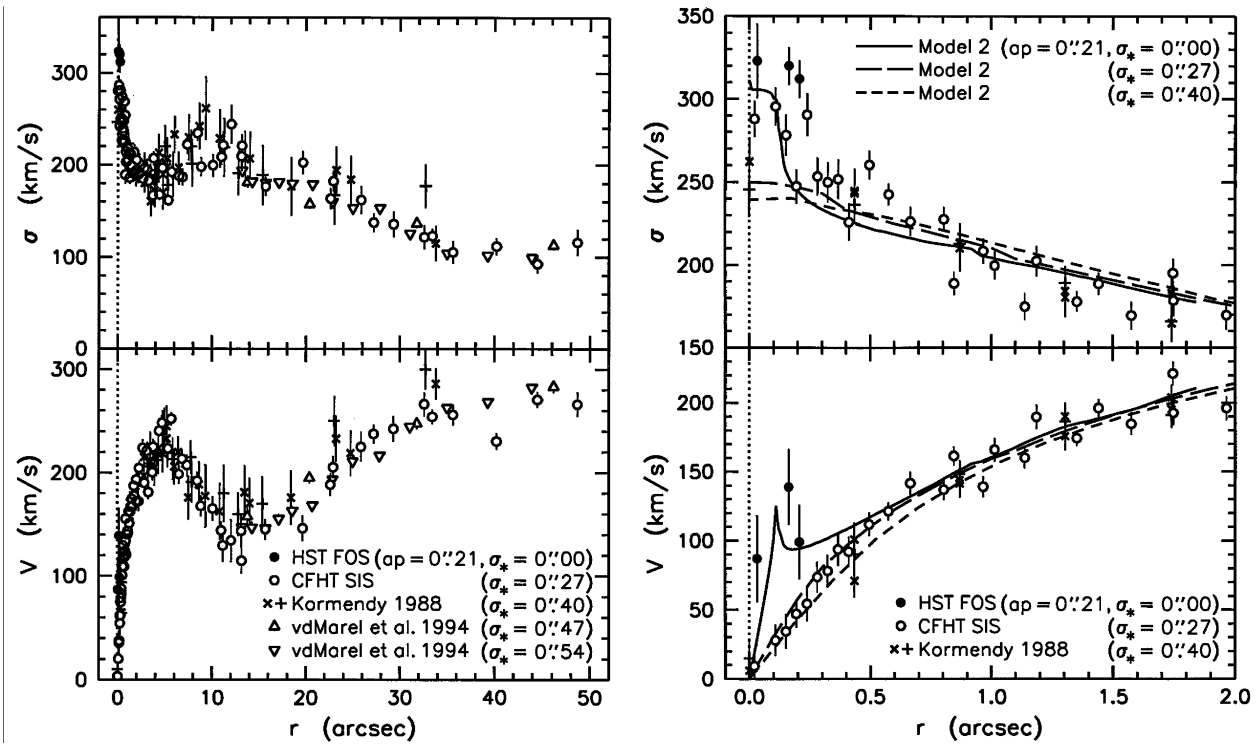

FIG. 2.—Major-axis kinematics of NGC 4594 as observed (*left*) and after subtraction of the bulge spectrum (*right*). The bulge spectrum was averaged at $|r| = 8''$–$13''$ and shifted to the systemic velocity; neglecting bulge rotation does not affect the results (K88). Bulge subtraction increases V and decreases σ by ~25 km s^{-1} at 2″, but it has essentially no effect near the center, so the *HST* velocities are not bulge-subtracted. The right-hand panel also shows model 2 from K88 as recomputed at SIS and *HST* resolution.

maximum V and σ values. They bracketed the observed kinematics after projection and seeing convolution, i.e., they provided high- and low-$M_\bullet$ error bars as well as good fits. All models implied that mass-to-light ratios increase rapidly at $r < 1''$ to values $M/L_V > 50$ that are much larger than those of old stellar populations. Two estimates of $M_\bullet$ were derived. If the M/L_V gradient is due to an MDO added to stars with constant $M/L_V(r)$, then $M_\bullet \simeq (1.8\text{–}4.4) \times 10^9\ M_\odot$. An alternative estimate is the mass interior to 0.″1: $M_\bullet \simeq (0.4\text{–}0.8) \times 10^9\ M_\odot$. K88 concluded that $M_\bullet \simeq 1 \times 10^9\ M_\odot$, with an estimated error of a factor of 3.

The K88 models were fitted to data with $\sigma_* = 0''.40$. We have recomputed them at SIS resolution ($\sigma_* = 0''.27$) and FOS resolution (0.″21 square aperture; $\sigma_* \simeq 0''.0$). The result is that all K88 models except model 2 are excluded by the *HST* data. They rotate too slowly near the center, and most do not show the rapid rise in σ at $r < 0''.3$. Only the highest-$M_\bullet$ model 2 in K88 approximately fits the *HST* data (Fig. 2, *right*). It has unprojected $\sigma = 265(r/1'')^{-1/2}$ km s^{-1}; $V \simeq 335$ km s^{-1} at large r, changing smoothly to $V = 380(r/1''.0)^{-1/2}$ km s^{-1} at $r < 2''$.

Model 2 has only slightly steeper kinematic gradients at $\sigma_* = 0''.27$ than at $\sigma_* = 0''.40$. It fits the SIS data as it did the K88 data, except that $\sigma(r \leq 0''.2)$ is about 40 km s^{-1} higher than predicted. High σ implies a large $M_\bullet$.

Model 2 is also a reasonable description of the *HST* data. At FOS resolution it shows the rapid rise to $V \simeq 110$ km s^{-1} at $r \simeq 0''.14$ and almost the correct high central $\sigma \simeq 321$ km s^{-1} seen in the observations. The reasonable agreement of a high-$M_\bullet$ isotropic model with data taken at resolution 5 times better than the σ_* for which it was derived confirms that the modeling techniques used in past BH papers are reliable (i.e., conservative in their implications about $M_\bullet$). Since only the model with the highest $M_\bullet$ is similar to the *HST* data, $M_\bullet$ is larger than K88 derived. On the other hand, we assume a smaller distance (9.2 Mpc versus 18.0 Mpc; see Kormendy & Richstone 1995). Therefore, we adopt $M_\bullet = 1 \times 10^9\ M_\odot$.

One limitation of model 2 deserves discussion. In the 1988 spectra, the sensitivity of the Fourier quotient program to line profile wings was limited by the accuracy of continuum subtraction. Model velocities were therefore restricted to $V \leq 500$ km s^{-1} and $\sigma \leq 300$ km s^{-1}. This does not imply that there are no higher velocity stars; in fact, the *HST* data show that such stars are present. Also, M/L_V had already risen by a factor of 4 outside the region where V and σ were set to constant values, so the detection of a dark object was robust. Still, the conclusion that this is a BH and not an extended cluster was less secure than in other galaxies. *HST* now shows steep kinematic gradients, supporting the conclusion that the dark object is a BH.

NGC 4594 is kinematically similar to NGC 3115 (K+96). In NGC 3115 the rotation curve is smoother (there is no dust) and $\sigma(r)$ rises more steeply inside $r = 0''.2$. The latter is due to the exceptionally hot stellar nucleus in NGC 3115. This provided a strong and independent argument for an MDO. We do not detect such a nucleus in NGC 4594 (§ 6), so NGC 3115 remains the stronger BH case.

5. EMISSION-LINE KINEMATICS

The detection of emission lines suggests that we try to measure $M_\bullet$ independently of the stellar kinematics. BH

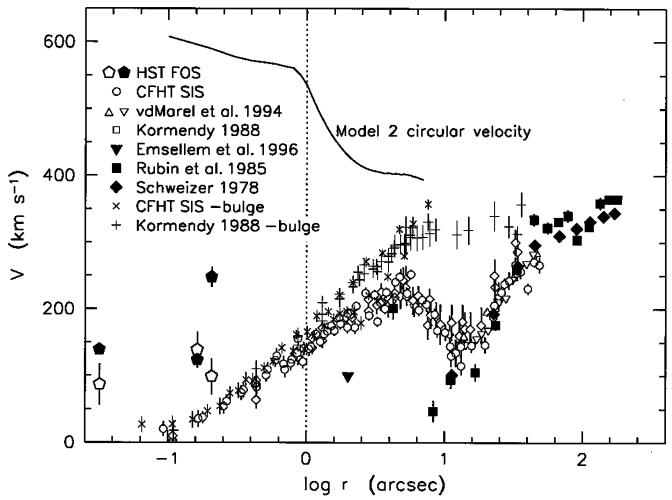

FIG. 4.—Major-axis velocities in NGC 4594 from emission lines (*filled symbols*) and absorption lines (*open symbols, plus signs, crosses*).

detections based on ionized gas velocities have been reported in M87 (Harms et al. 1994) and in NGC 4261 (Ferrarese, Ford, & Jaffe 1996). Unfortunately, gas can also fail to measure masses; NGC 4594 is an example.

Figure 3 (Plate L14) shows the emission-line spectrum after a model of the absorption-line spectrum has been subtracted. NGC 4594 is a mini-Seyfert (Filippenko & Sargent 1985); with our small aperture, dilution by light from the rest of the galaxy is minimal and the broad lines dominate the spectrum. The Hα line has FWZI $\simeq$ 5200 km s^{-1}.

We measured velocities using the narrow lines. This reveals two problems. First, different lines give different velocities (Fig. 3, *bottom*). Most lines agree, but one or two are discrepant, and different lines are discrepant in different apertures. To illustrate the second problem, Figure 4 plots $V(r)$ for the lines that agree with each other. The gas rotates more rapidly in the nuclear disk than at $r \simeq 10''$ (see also Rubin et al. 1985). But the gas velocities are much smaller than the circular velocities implied by the stars (*solid line*). The same is true at larger radii (Kormendy & Westpfahl 1989; Emsellem et al. 1996). In fact, between the nuclear and main disks, the gas velocities are smaller than the stellar velocities. But the latter must be smaller than the circular velocity because σ is large (see the bulge-subtracted velocities in Fig. 4 ["− bulge"], which have $\sigma \simeq 100$ km s^{-1} at $r \gtrsim 10''$ and so are closer to circular). Possible reasons are discussed in the above papers; the simplest is that the gas may be in a ring at relatively large radii. The slow rotation is worth further study, but it does mean that the gas velocities do not constrain $M_\bullet$.

6. THE NONTHERMAL NUCLEUS

Figure 1 shows that NGC 4594 has an apparent nucleus. Is this a star cluster, or is it a nonthermal source? Absorption-line strengths tell us the answer. Since σ is the same for all three apertures, Figure 1 (*bottom*) shows that the absorption lines look weaker when the nucleus is included. If the true line strengths are the same in all apertures, then the measured equivalent widths of Mg b, Fe λ5270, and Fe λ5335 imply that nonthermal flux makes up 50% $\pm$ 15% of the light in the central aperture. This accounts for the extra brightness in the central four pixels (Fig. 1). To check this result, we subtracted the spectrum at $r = 0''.163$ from that at $r = 0''.032$. These apertures overlap, but only the latter contains the nucleus. In the difference spectrum, the absorption lines have vanished. This confirms that the central point source is not made of old stars. There is a small possibility that it is made of young, blue stars. But it is more likely to be nonthermal and part of the nuclear activity. The $V - I$ image in Figure 1 shows that the nucleus is not bluer than the bulge. But there are reddened patches on either side of it, so it may be reddened, too.

We conclude that NGC 4594 is similar to M87, an active galaxy in which the central point source is nonthermal (Dressler 1989; Dressler & Richstone 1990; Kormendy 1992) and not to M31 and NGC 3115, which contain nuclear star clusters and apparently quiescent BHs.

We are most grateful to C. D. Keyes, J. Christensen, and J. Hayes for help with the data analysis. This work was supported by *HST* data analysis funds through grant GO-02600.01-87A and by NSERC. Kormendy's ground-based work was supported by NSF grant AST-9219221; Bender was supported by SFB 375 and by the Max-Planck-Gesellschaft.

REFERENCES

Bender, R. 1990, A&A, 229, 441
Burkhead, M. S. 1986, AJ, 91, 777
———. 1991, AJ, 102, 893
Carter, D., & Jenkins, C. R. 1993, MNRAS, 263, 1049
Dressler, A. 1989, in IAU Symp. 134, Active Galactic Nuclei, ed. D. E. Osterbrock & J. S. Miller (Dordrecht: Kluwer), 217
Dressler, A., & Richstone, D. O. 1990, ApJ, 348, 120
Emsellem, E., Bacon, R., Monnet, G., & Poulain, P. 1996, A&A, 312, 777
Emsellem, E., Monnet, G., Bacon, R., & Nieto, J.-L. 1994, A&A, 285, 739
Ferrarese, L., Ford, H. C., & Jaffe, W. 1996, ApJ, 470, 444
Filippenko, A. V., & Sargent, W. L. W. 1985, ApJS, 57, 503
Harms, R. J., et al. 1994, ApJ, 435, L35
Jarvis, B. J., & Dubath, P. 1988, A&A, 201, L33
Keyes, C. D., et al. 1995, FOS Instrument Handbook (Baltimore: STScI)
Kormendy, J. 1988, ApJ, 335, 40 (K88)
———. 1992, ApJ, 388, L9
———. 1994, in The Nuclei of Normal Galaxies, ed. R. Genzel & A. I. Harris (Dordrecht: Kluwer), 379
Kormendy, J., et al. 1996, ApJ, 459, L57 (K+96)
Kormendy, J., & Richstone, D. 1992, ApJ, 393, 559
———. 1995, ARA&A, 33, 581
Kormendy, J., & Westpfahl, D. J. 1989, ApJ, 338, 752
Rubin, V. C., Burstein, D., Ford, W. K., & Thonnard, N. 1985, ApJ, 289, 81
Schweizer, F. 1978, ApJ, 220, 98
van der Marel, R. P., Rix, H.-W., Carter, D., Franx, M., White, S. D. M., & de Zeeuw, T. 1994, MNRAS, 268, 521
Wagner, S. J., Dettmar, R.-J., & Bender, R. 1989, A&A, 215, 243

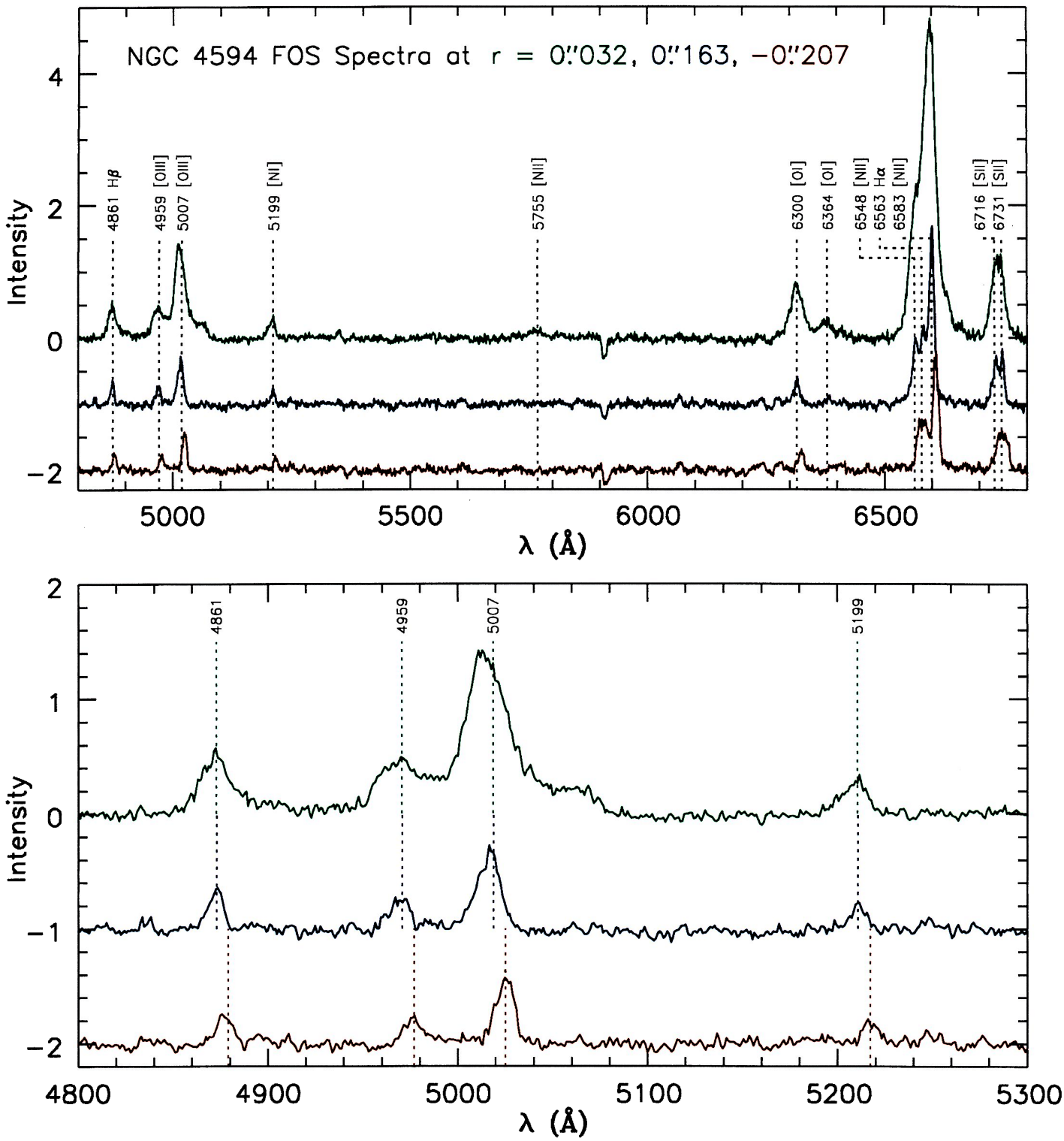

FIG. 3.—FOS emission-line spectra of NGC 4594, color coded as in Fig. 1. The underlying absorption-line spectra have been removed as in Filippenko & Sargent (1985): we subtracted an emission-line–less spectrum of a standard galaxy (NGC 3379) that had been velocity-shifted, broadened, and intensity-scaled to match the absorption-line spectrum of NGC 4594. All lines subtract well except Na I D λ5892; we ascribe this to interstellar absorption. In the top panel, essentially the whole wavelength range is shown; the Seyfert characteristics discussed by Filippenko & Sargent (1985) are prominent. The dotted lines are plotted at the mean velocity adopted for the $r = 0.''032$ spectrum. The bottom panel shows Hβ, [O III] λλ4959, 5007, and [N I] λ5199. Dotted lines indicate the adopted mean velocity at each radius. In the $r = 0.''032$, $0.''163$, and $-0.''207$ spectra, λλ5007, 5007, and 4861, respectively, do not agree with the mean velocities derived from the other emission lines.